

Saturable absorption in multi-core fiber couplers

Elham Nazemosadat and Arash Mafi*

*Department of Electrical Engineering and Computer Science,
University of Wisconsin-Milwaukee, Milwaukee, WI 53211, USA*

(Dated: 26 July 2013)

The saturable absorption characteristics of two-, three-, and five-core one-dimensional fiber coupler arrays and the seven-core hexagonal fiber coupler array are investigated. It is shown that the performance of all these saturable absorbers are comparable and not much is gained, if anything, by going from a two-core nonlinear coupler geometry to a higher number of cores. This observation is supported by the similarity of the saturable absorption curves, as well as comparable pulse characteristics obtained from the simulation of a generic mode-locked fiber laser cavity.

PACS numbers: 42.81.Qb, 42.55.Wd, 42.65.Re, 42.65.Tg, 42.65.Jx, 42.65.Pc

The operation of a mode-locked laser requires a form of intensity discrimination otherwise known as saturable absorption¹. Common saturable absorbers (SA) include semiconductor SA mirrors (SESAM)², carbon nanotubes³, graphene⁴, Kerr lensing⁵, and nonlinear polarization rotation (NPR)⁶. Desired attributes of SAs include fast response time (relaxation time), stability, long-term reliability, ease of use, appropriate saturation fluence, and low loss⁷.

For mode-locked fiber laser applications, fully integrable SAs are desired in order to take full advantage of a robust alignment-free fiber cavity. Common fiber-integrable SA solutions have deficiencies that limit their usefulness for mode-locked fiber laser applications: SESAMs generally have picosecond response times, making them less desirable for ultrashort pulse generation, and their nonsaturable losses can result in excessive heating⁸. The long-term reliability of carbon nanotube- and graphene-based SAs when exposed to intense optical pulses is at best questionable⁹, and both are limited in modulation depths. SAs based on nonlinear polarization rotation are very sensitive to the slightest perturbation of the fiber cavity, making them unsuitable outside the laboratory.

Another problem with the present SA technology concerns the rapid growth in the maximum achievable pulse energy and peak power in mode-locked fiber lasers over the past decade¹⁰⁻¹². SAs are becoming a limiting factor in scaling up the pulse energy and peak power to higher values. SESAMs, carbon nanotubes, and graphene will likely not be suitable for ultrahigh pulse energies due to heat generation and long-term reliability. The periodic SA curve in a nonlinear polarization rotation SA with respect to the pulse power and its sensitivity to environmental perturbations makes this technique unsuitable for ultrahigh-peak-power mode-locked lasers.

Nonlinear mode coupling in waveguide arrays (NMCWA), including multi-core fiber implementations, offers an attractive alternative that addresses most of the limitations faced by common SAs. A dual-core fiber laser geometry as an embedded SA was originally proposed by Winful et al.¹³. Since then, several theoretical studies have been conducted on nonlinear mode coupling in semi-

conductor coupled waveguide arrays¹⁴⁻¹⁶, and multi-core optical fibers^{17,18}. More recently, a seven-core tapered optical fiber was explored in the nonlinear regime and it was shown to have the potential to be used as an SA¹⁹.

A mode-locked fiber laser using an AlGaAs waveguide array SA was recently demonstrated experimentally²⁰. This demonstration clearly serves as a convincing experimental proof-of-concept for the potential application of NMCWA as an SA. However, for practical device applications and improved efficiency, the insertion loss of the waveguide array needs to improve. An all-fiber SA in the spirit of Refs.^{13,17,18} seems like an ideal solution to the insertion loss problem, because it can be easily spliced to other components in the fiber cavity. Although semiconductor arrays benefit from a larger nonlinear coefficient resulting in desirably short SAs, fibers made from chalcogenide glasses with nonlinear coefficients of up to 1000 times larger than silica can provide similar performances^{21,22}. In addition, the nearly instantaneous response of nonlinearities in optical fibers is ideal for ultrashort pulse generation^{22,23}.

In this paper, we study the performance of the multi-core SAs as a function of the number of the waveguide cores. Many-core geometries have been the center of attention in NMCWA SAs; e.g., the NMCWA studied in Ref.¹⁴ has 41 coupled waveguides. We explore and compare the saturable absorption characteristics of two-, three-, and five-core one-dimensional (1D) arrays and the seven-core hexagonal array illustrated in Fig. 1. The main question that is addressed in this paper is whether increasing the number of the cores improves the saturable absorption characteristics of these nonlinear multi-core arrays.



FIG. 1: The two-, three-, and five-core 1D arrays and the seven-core hexagonal array are shown in a fiber-optic geometry. All cores are assumed to be identical in a given geometry. The launch core is identified with a darker shade.

The results indicate that the performance of all these SAs are comparable and not much is gained, if anything, by going from a two-core nonlinear coupler geometry to a higher number of cores. This observation is supported by the similarity of the saturable absorption curves, as well as comparable pulse characteristics obtained from the simulation of a generic mode-locked fiber laser cavity. In the latter case, these SAs are placed in a fiber laser cavity, in which self-starting stable mode-locked pulses are generated. According to the results, one can benefit from the simpler setup of a two-core fiber with optimized parameters to get the desired output mode-locked pulses instead of using the more complex multi-core fibers.

In the following, for each multi-core fiber SA in Fig. 1, the optical beam is launched in the *launch core* identified with a darker shade and is collected from the same core at the other end after propagating through the length of the SA. The dependence of the transmission through the multi-core fiber on the optical power serves as the desired saturable absorption mechanism.

In the linear regime where optical power is low, neighboring waveguides exchange optical power periodically; the linear coupling is caused by the modal overlap of adjacent waveguides and is most efficient when the adjacent modes have identical propagation constants²⁴. In Fig. 2, the transmission through the multi-core arrays of Fig. 1 is shown in the linear regime as a function of the normalized length L relative to \tilde{c}^{-1} ; \tilde{c} is the linear coupling coefficient between adjacent cores and is assumed to be the same among all neighboring cores in a given geometry. The half-beat-length L_c is defined as the distance over which the energy is maximally exchanged from the launch core to the neighboring cores and depends on the number of fiber cores and the geometry.

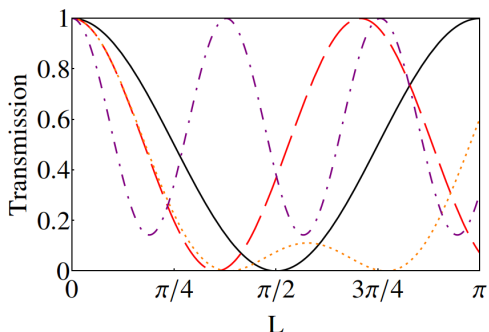


FIG. 2: The transmission through the two-core (solid black), three-core (dashed red), five-core (dotted orange) fiber 1D arrays and the seven-core hexagonal array (dash-dotted purple) is shown as a function of the normalized length in the linear regime.

It can be seen that the half-beat-length of a three-core fiber is shorter than the two-core fiber, because its launch core is coupled to “more” side cores with the same strength and can exchange the optical power more efficiently. The linear dynamics in the case of five cores is a bit more complex due to the differing power exchange

efficiencies of the side cores, but the first minimum happens for only a slightly longer SA device. In the case of the seven-core hexagonal array, the central core couples to six cores in the outer ring, resulting in a rapid exchange of optical power and shorter half-beat-length; however, the power in the central core always remains larger than zero where the minimum value of transmission is $1/7 \approx 14.3\%$. In all these cases, the half-beat-length is inversely proportional to the coupling strength and is given by $\tilde{c}L_c = \xi_n(\pi/2)$, where ξ_n is a numerical coefficient for the n -core scenarios studied here. We have $\xi_2 = 1$, $\xi_3 = 1/\sqrt{2} \approx 0.71$, $\xi_5 = 4/\sqrt{27} \approx 0.77$, and $\xi_7 \approx 0.378$.

In the nonlinear regime where optical power is high, self-phase and cross-phase modulation (SPM and XPM) effects alter the refractive index of each waveguide and consequently detune the effective propagation constants of the modes, reducing the power exchange efficiency between adjacent cores²⁵. In other words, if high power is launched into a waveguide, the effective couplings to neighboring cores are reduced and the light remains mainly in the launch core. If the total length of the coupler in each case is chosen to be equal to the half-beat-length, for an optical pulse transmitting through the fiber array, its low intensity sides are efficiently channeled to the adjacent cores, while its high intensity center peak remains in the launch core, resulting in a power-dependent transmission and intensity discrimination^{13,14}. This saturable absorption feature can be used to produce the required pulse shaping for stable and robust mode-locked pulse trains.

The differential equation describing the propagation of the electric field in the n th core of a multi-core fiber nonlinear coupler, where only the interactions between the nearest neighbors are considered, is given by

$$\frac{\partial E_n}{\partial \zeta} = i \sum_{\tilde{n}} E_{\tilde{n}} + i \tilde{\gamma}_n |E_n|^2 E_n + i \sum_{\tilde{n}} \mu_{n,\tilde{n}} |E_{\tilde{n}}|^2 E_n. \quad (1)$$

E_n is the electric field envelope normalized to the pulse peak power P_0 at the entrance of the launch core. The \tilde{n} sums are over the cores adjacent to the n th core. The propagation distance is rescaled to $\zeta = \tilde{c}z$. $\tilde{\gamma}_n = \gamma_n^* P_0 / \tilde{c}$ is a dimensionless parameter characterizing the nonlinear strength, where γ_n^* is the SPM coefficient of the n th core and $\mu_{n,\tilde{n}}$ is the cross-phase modulation coefficient between the n th core and the adjacent cores. The XPM terms are much smaller than the SPM terms and are thus neglected, i.e., $\mu_{n,\tilde{n}} \approx 0$. The dispersion and loss of the fiber coupler can be neglected if the SA length is sufficiently smaller than its dispersion length and effective length²³.

The nonlinear consequences of the coupled beam propagation in multi-core arrays have been previously explored in detail; e.g., in Ref.²⁶. Here, we borrow from these studies to obtain the saturable absorption curves of the multi-core arrays of Fig. 1. The length of each SA array is assumed to be equal to the half-beat-length to ensure minimum transmission in the low-power linear

regime. The saturable absorption curves are shown in Fig. 3 where the transmission through the launch core of the multi-core SA array is plotted as a function of the normalized nonlinear strength $\tilde{\gamma}$, which is assumed to be the same for all cores. The saturable absorption is dictated by a competition between the linear coupling term $i \sum_{\bar{n}} E_{\bar{n}}$ versus the nonlinear SPM term $i\tilde{\gamma}_n |E_n|^2 E_n$ in Eq. 1 and the transition from low transmission to high transmission occurs when these two terms are comparable.

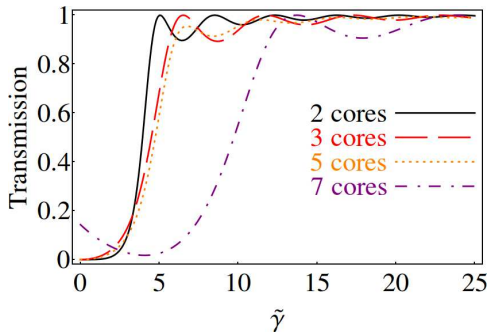


FIG. 3: Nonlinear transmission through a two-core (solid black), three-core (dashed red), five-core (dotted orange) fiber 1D arrays and the seven-core hexagonal array (dash-dotted purple) is shown as a function of the normalized nonlinear strength $\tilde{\gamma}$, which is assumed to be the same for all cores. The length of each SA array is chosen to be equal to the half-beat-length.

The three-core fiber SA has two adjacent cores coupled to its launch core and consequently has a larger linear coupling term compared with the two-core scenario; therefore, more optical power (larger SPM term) is required to overcome the linear coupling term. That is why the three-core SA requires slightly higher power for nonlinear saturation. The five-core and three-core scenarios are nearly identical, because even in the five-core scenario, the launch core is only adjacent to two neighboring cores. The saturable absorption curves for a higher number of cores in 1D linear arrays are practically identical to the five-core SA.

For the seven-core hexagonal array SA, the nonlinear SPM term must overcome the linear coupling to six adjacent cores and requires higher normalized nonlinearity to saturate the SA. However, the SA curve closely resembles those of 1D arrays and can be mapped to the 1D saturable absorption curves by adjusting the core-to-core \tilde{c} coefficient. In fact, if SA devices are chosen at the same length, where \tilde{c} must inevitably be smaller for the seven-core array, the saturable absorption curves for all the geometries in Fig. 1 will be nearly identical as a function of the input power. This can easily be seen if the “horizontal scale” for the seven-core SA curve in Fig. 1 is rescaled by a factor of approximately 2/6 to compensate for the six adjacent cores versus the two adjacent cores in the three-core fiber. The SA curves nearly overlap after such a rescaling. This fact will result in nearly identical

pulse characteristics in mode-locked cavity simulations of Fig. 4, as will be discussed shortly.

There is another notable difference in the seven-core saturable absorber: the transmission initially drops to zero at finite $\tilde{\gamma}$ before saturating at higher power. This effect is due to the complex coupling pattern in the seven-core geometry. A nearly monotonic increase can be artificially created by shortening the fiber below the half-beat-length at the expense of a smaller modulation depth.

To study the mode-locking behavior of the multi-core array, it is placed within the mode-locking optical cavity. A typical passive mode-locked fiber laser consists of an active single mode fiber with a bandwidth-limited gain, which compensates for the energy loss in the cavity, and an intensity discrimination device as an SA. When the interactions of the attenuation, chromatic dispersion, nonlinearity, and bandwidth-limited gain in the optical fiber cavity are combined with the intensity discrimination, a train of mode-locked pulses is formed from white noise after several numbers of round trips in the cavity. These interactions are captured by two sets of equations: one is the nonlinear Schrödinger equation governing the pulse propagation in the cavity, while the other is Eq. 1 describing the saturable absorption.

The pulse propagation in the cavity is given by²⁷

$$\frac{\partial A}{\partial z} = -\alpha A + \frac{i}{2} \frac{\partial^2 A}{\partial T^2} + i\eta |A|^2 A + g(z)(1 + \tau \frac{\partial^2}{\partial T^2})A, \quad (2)$$

where $A(z, T)$ is the normalized electric field envelope, z is the propagation distance along the fiber, and T represents the time measured in the retarded frame of the pulse normalized by a constant T_0 , which is the expected pulse duration. $A(z, T)$ is normalized by the peak power of the fundamental soliton $P_{fs} = |\beta_2|/(\gamma T_0^2)$, where β_2 is the group velocity dispersion of the fiber, and γ is the fiber nonlinear coefficient²³.

It is also implicitly assumed that the wavelength of the pulse $\lambda_0 = 1.55 \mu\text{m}$ falls within the anomalous-dispersion regime of the fiber. The propagation distance z is scaled to the dispersion length $L_D = T_0^2/|\beta_2|$, and η is the dimensionless cavity nonlinear coefficient given by $\eta = \gamma P_{fs} L_D$. The normalized attenuation is considered through α , while the bandwidth-limited gain of the cavity is described by the parameters $g(z)$ and τ . The dimensionless parameter τ controls the pulse width in the mode-locking process and is given by $\tau = 1/(\Delta\omega T_0)^2$ where $\Delta\omega = (2\pi c/\lambda_0^2)\Delta\lambda$ is the spectral gain bandwidth and $\Delta\lambda$ is the gain bandwidth²⁸. The gain saturation $g(z)$ is given by

$$g(z) = \frac{2g_0}{1 + \|A\|^2/e_0}, \quad (3)$$

where g_0 and e_0 are the pumping strength and the cavity saturation energy, respectively, and $\|A\|^2 = \int_{-\infty}^{\infty} |A|^2 dT$ is the pulse energy.

The simulations are based on Eq. 2, while Eq. 1 is applied in every round trip of the laser cavity. The coupling

efficiency of the cavity to the launch core of the multi-core SA is assumed to be 100% on both the entrance and the exit ports; therefore, A in Eq. 2 becomes E at the entrance in the launch core of the multi-core geometry in Eq. 1 and vice versa at the exit.

For the mode-locking cavity simulations, the initial pulse conditions are assumed to be low amplitude noise fluctuations. The cavity length is 5m, while the rest of the parameters used are $T_0 = 114$ fs, $\alpha = 0.05$, $\Delta\lambda = 35$ nm, $g_0 = 0.39$ and $e_0 = 1^{28}$. We also have $\beta_2 = -0.0153$ ps²/m resulting in $L_D = 0.84$ m. The nonlinear coefficient of the cavity is chosen as $\gamma = 1.7$ km⁻¹W⁻¹. The nonlinear coefficient of the SA is assumed to be $\gamma^* = 0.34$ m⁻¹W⁻¹, which can be obtained by using a chalcogenide glass fiber²¹.

Fig. 4 shows the normalized power of the mode-locked pulses after 100 round trips in the laser cavity, resulting in full convergence, as a function of the length the SA. For each length (and for each SA), the core-to-core coupling coefficients \tilde{c} are adjusted so that the length of the SA is equal to the half-beat-length for optimum performance. This choice of the coupling coefficients ensures that the power is maximally transferred from the launch core to the other cores in the linear regime. In practice, the core-to-core coupling coefficients \tilde{c} can be designed and controlled via core-to-core separations. As we discussed above, the saturable absorption curves for all multi-core arrays studied here are nearly identical when the SAs are of the same length. Therefore, it should come at no surprise that the normalized pulse peak power is nearly the same for all these SAs as shown in Fig. 4.

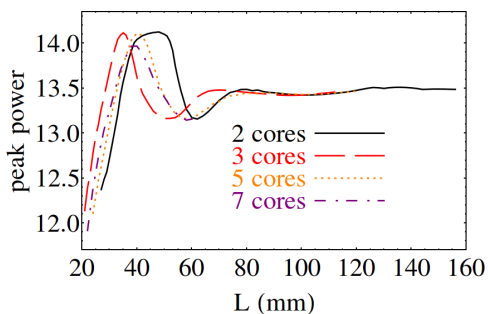


FIG. 4: The normalized peak power of the mode-locked pulses are shown as a function of the length the SA, where the core-to-core coupling coefficients c are adjusted so that the length of the SA is equal to the half-beat-length.

In summary, the results in Figs. 3 and 4 show that nearly identical performance is expected from the geometries that we explored. While that results are seemingly generic for popular SA geometries, we emphasize that this study is not exhaustive. An infinite number of multi-core geometries can be constructed even with non-uniform core-to-core couplings and non-identical core sizes applied to many different choices of laser parameters. Therefore, the main conclusion one can draw from this study is that when an NMCWA is to be used as an SA, it is important to verify whether multiple cores yield any tangible performance benefits besides making the device unnecessarily more complex. Future efforts will focus on comparisons between multi-mode and multi-core all-fiber SA devices²⁹.

Acknowledgments

The authors acknowledge support from the Air Force Office of Scientific Research under Grant FA9550-12-1-0329.

* corresponding author.

¹ B. K. Garside and T. K. Lim, *J. Appl. Phys.* **44**, 2335 (1973).
² U. Keller et al., *IEEE J. Sel. Top. Quantum Electron.* **2**, 435–453 (1996).
³ Sze Y. Set, H. Yaguchi, Y. Tanaka, and M. Jablonski, *J. Lightwave Technol.* **22**, 51–56 (2004).
⁴ T. Hasan et al., *Adv. Mater.* **21**, 3874–3899 (2009).
⁵ D. E. Spence, P. N. Kean, and W. Sibbett, *Opt. Lett.* **16**, 42–44 (1991).
⁶ D. U. Noske, N. Pandit, and J. R. Taylor, *Electron. Lett.* **28**, 2185–2186 (1992).
⁷ M. Haiml, R. Grange, and U. Keller, *Appl. Phys. B* **79**,

331–339 (2004).

⁸ R. Paschotta et al., *Appl. Phys. B* **70**, S25–S31 (2000).
⁹ Y. W. Song, S. Yamashita, and S. Maruyama, *Appl. Phys. Lett.* **92**, 021115–021115-3 (2008).
¹⁰ B. Ortac, M. Baumgartl, J. Limpert, and A. Tunnermann, *Opt. Lett.* **34**, 1585–1587 (2009).
¹¹ S. Lefrancois, K. Kieu, Y. Deng, J. D. Kafka, and F. W. Wise, *Opt. Lett.* **35** 1569–1571 (2010).
¹² S. Lefrancois, C.-H. Liu, M. L. Stock, T. S. Sosnowski, A. Galvanauskas, and F. W. Wise, *Opt. Lett.* **38** 43–45 (2013).
¹³ H. G. Winful, and D. T. Walton, *Opt. Lett.* **17**, 1688–1690 (1992).

- ¹⁴ J. L. Proctor, and J. N. Kutz, *Opt. Lett.* **30**, 2013–2015 (2005).
- ¹⁵ H. S. Eisenberg, Y. Silberberg, R. Morandotti, A. R. Boyd, and J. S. Aitchison, *Phys. Rev. Lett.* **81**, 3383–3386 (1998).
- ¹⁶ D. D. Hudson, K. Shish; T. R. Schibli, J. N. Kutz, D. N. Christodoulides, R. Morandotti, and S. T. Cundiff, *Opt. Lett.* **33**, 1440–1442 (2008).
- ¹⁷ S. R. Friberg, A. M. Weiner, Y. Silberberg, B. G. Sfez and P. S. Smith, *Opt. Lett.* **13**, 904–906 (1988).
- ¹⁸ A. Betlej, S. Suntsov, K. G. Makris, L. Jankovic, D. N. Christodoulides, G. I. Stegeman, J. Fini, R. T. Bise and D. J. DiGiovanni, *Opt. Lett.* **31**, 1480–1482 (2006).
- ¹⁹ Thomas F. S. Büttner, Darren D. Hudson, Eric C. Mägi, Alvaro Casas Bedoya, Thierry Taunay, and Benjamin J. Eggleton, *Opt. Lett.* **37**, 2469–2471 (2012).
- ²⁰ Q. Chao, D. D. Hudson, J. N. Kutz, and S. T. Cundiff, *IEEE Photon. J.* **4**, 1438–1442 (2012).
- ²¹ G. Lenz et al., *Opt. Lett.* **25**, 254–256 (2000).
- ²² N. Sugimoto, H. Kanbara, S. Fujiwara, K. Tanaka, Y. Shimizugawa, and K. Hirao, *J. Opt. Soc. Am. B* **16**, 1904–1908 (1999).
- ²³ G. P. Agrawal, *Nonlinear fiber optics*, 5th ed. (Elsevier Science, 2013).
- ²⁴ B. E. A. Saleh, and M. C. Teich, *Fundamentals of Photonics*, 2nd ed. (Wiley, 2007).
- ²⁵ S. M. Jensen, *IEEE J. Quantum Electron.* **18**, 1580–1583 (1982).
- ²⁶ D. N. Christodoulides, and R. I. Joseph, *Opt. Lett.* **13**, 794–796 (1988).
- ²⁷ H.A. Haus, *IEEE J. Sel.Top. Quant. Elec.* **6**, 1173–1185 (2000).
- ²⁸ J. L. Proctor, and J. N. Kutz, *Opt. Express* **13**, 8933–8950 (2005).
- ²⁹ E. Nazemosadat and A. Mafi, *J. Opt. Soc. Am. B* **30**, 1357–1367 (2013).